Research Article

Journal of Environmental Nanotechnology

Eco-friendly Production of Zinc Oxide Nanoparticles via *Morinda citrifolia* for Solar-driven Photocatalytic Decomposition of Malachite Green Dye

D. Tamilselvi[1*], K. Rathidevi[2], N. Chithra[3] and R. Nandhini[1]

[1]Department of Science and Humanities, Rathinam Technical Campus, Coimbatore, TN, India
[2]Department of Chemistry, Kumaraguru College of Technology, Coimbatore, TN, India
[3]Department of Chemistry, Dr. Mahalingam College of Engineering and Technology, Pollachi, TN, India
Received: 17.04.2025 Accepted: 23.09.2025 Published: 30.09.2025
*tamilselviupdate@gmail.com

ABSTRACT

The manufacture of metal oxide nanoparticles using extracts from medicinal plants offers a viable and environmentally responsible substitute for conventional chemical methods. This work aims to utilize the leaf extract of the medicinal plant *Morinda citrifolia* (Noni) to synthesize zinc oxide nanoparticles in an eco-friendly manner. The zinc oxide nanoparticles obtained through biosynthesis underwent characterization using various analytical techniques, including XRD, SEM, EDX, FTIR, and UV spectroscopy. Moreover, this investigation included an assessment of the photoluminescent activity of the synthesized zinc oxide nanoparticles under varying excitation wavelengths. The observed emission in the visible region finds significant applications in opto-electronic devices, particularly for display purposes. Sunlight-driven photocatalytic degradation efficiency exceeding 90% was achieved within a 60-minute timeframe under sunlight irradiation.

Keywords: Zinc oxide; *Morinda citrifolia* (Noni leaf); Photocatalytic activity; Malachite green dye.

1. INTRODUCTION

Nanoparticle (NP) production using plant extracts is a rapidly developing, eco-friendly approach with diverse applications in medicine, food, industry, and agriculture. Plant-based NPs have clear advantages over NPs made using traditional methods, which frequently exhibit toxicity, specifically in the clinical sector. The physicochemical properties of plant-synthesized NPs provide an extended lifespan, addressing the limitations associated with conventional chemical and physical synthesis methods (Kavitha *et al*. 2012; Amna *et al*. 2015; Malik *et al*. 2014; Kalpana and Devi, 2018). Plants are highly genetically variable and produce a broad scope of metabolites and biomolecules, including vitamins, proteins, flavonoids, phenols, carbohydrates, and coenzyme-based intermediates. Plant-derived metabolites facilitate the reduction process, converting metal ions to the nanoscale, attributed to the existence of functional groups such as hydroxyl, carbonyl, and amine. In particular, the –OH groups in flavonoids serve as a pivotal factor in transforming metal ions into nanomaterials (Makarov *et al*. 2014). The metal selected for NPs biosynthesis has a significant impact on its end-use industry. While plant extracts from various species have been extensively utilized to synthesize nanoparticles (NPs) of metals such as Ag, Cu, and Au, concerns over their elevated toxicity have limited their application in the medical field (Mittal *et al*. 2013; Ahmed *et al*. 2016).

In contrast, zinc oxide (ZnO) is an inorganic substance that is mostly noticed in crystalline form and is found in nature infrequently. Pure zinc oxide is a white powder and is water-insoluble in nature. Zinc oxide NPs are extensively employed in cosmetics, textiles, diagnostics, and microelectronics because of their less toxic nature and size-dependent characteristics (Fan *et al.* 2013). Zinc oxide NPs have a great possibility to cure infectious disorders in animals and humans because they are generally recognized as safe (GRAS) designation and natural antibacterial characteristic (Sushma *et al.* 2016). In comparison to other metals, ZnO has also proven to be particularly useful and efficient for the biosynthesis of NPs intended for medical applications. Numerous research works have supported the effective production of ZnO NPs from a variety of plant extracts. For example, the leaf extract of *Hibiscus rosa-sinensis* (Ramesh *et al*. 2015) and the blossom extract of *Cassia auriculata* (Divya and Nithya, 2015) were utilized to create ZnO NPs by reducing zinc nitrate.

A range of methods has been developed for wastewater treatment, including adsorption, coagulation, sedimentation, filtration, chemical oxidation, and photocatalysis. Among these, photocatalysis has

garnered considerable focus owing to its proficiency to completely mineralize toxic pollutants into innocuous end products like water and carbon dioxide (Jo and Tayade, 2014; Dong *et al.* 2015). This approach, applicable to both liquid and gaseous phases, can harness abundant solar energy by operating under low-intensity temperature and pressure conditions, and is non-selective toward specific compounds.

Among metal oxide catalysts, ZnO is recognized as a highly efficient photocatalyst owing to its wide band gap, low cost, minimal energy requirements, and non-toxic nature (Lee *et al.* 2016). Plant extracts offer a sustainable route for ZnO synthesis, as they enable rapid production with low resource input, natural compound dispersion, cost-effectiveness, and high stability, while ensuring safe handling. Bioactive phytoconstituents in plants serve a dual purpose, reducing metal ions and preventing particle aggregation through stabilization, facilitating nanoparticle formation, and preventing agglomeration during synthesis.

Additionally, the biomolecules within the extracts can enhance the electron release mechanism in photocatalysis, thus enhancing the catalytic efficiency of nanoparticles. Hence, plant-extract-mediated green synthesis provides an environmentally benign pathway for nanoparticle production, utilizing the bioactive constituents as both stabilizers and reductants (Vivek *et al*. 2019; Wan *et al*. 2020).

Plant-based green synthesis technologies offer many advantages over traditional methods. These include reduced environmental impact, lower toxicity, cost-effectiveness, and the use of renewable resources. Plant extracts act as natural reductants and stabilizers, removing the need for harmful chemicals. Moreover, this approach facilitates electron donation during photocatalytic reactions, thereby improving the catalytic performance of nanoparticles. Consequently, plant-mediated green synthesis emerges as a sustainable and promising strategy for the formulation of metal oxide nanoparticles. This highlights the potential benefits and effectiveness of ZnO in the biosynthesis of NPs for medical applications (Al-darwesh *et al*. 2024).



Fig. 1: *Morinda citrifolia* leaves: a) Fresh and b) Dried

1.1 *Morinda citrifolia* (Noni) Leaves

Noni leaf tea has very few negative effects and a vast potential for treating a variety of health and wellness issues. Its unique applications and characteristics are listed below.

1.2 Uses

The noni tree is an evergreen with large leaves and yellow fruit. It is found in India, Australia, Southeast Asia, and the Pacific Islands. The entire noni plant—roots, stem, bark, leaves, flowers, and fruit—has been utilized for medicinal purposes. Particularly, fruit juice has a relatively high potassium content. It has several additional compounds, including vitamins A and C, that may aid in the body's ability to heal damaged cells and stimulate the immune system.

1.3 Qualities

With an extensive scope of advantageous characteristics, including antioxidant, anti-fungal, anti-inflammatory, antibacterial, anodyne, and nutritional benefits, the noni leaf stands out as a super-herb. Amongst the alkaloids found in the *Morinda citrifolia* plant, Heinicke *et al.* (1985) observed significant concentrations of proxeronine, the precursor of xeronine. The author claims that xeronine has a multitude of biological actions and functions, including changing the molecular structure of proteins. Xeronine aids in the restructuring of molecules to their active conformation when an enzyme, protein, or cellular signal receptor lacks its proper configuration. Additionally, the presence of xeronine contributes to various health benefits, including the alleviation of conditions such as atherosclerosis, menstrual cramps, depression, and hypertension (Lee *et al*. 2016; Shengmin *et al.* 2002).

Zinc oxide, classified as a II–VI semiconductor material, possesses a bandgap of 3.37 eV. Well-known for its unique physicochemical properties, including stability towards chemicals and a broad range of light absorption, zinc oxide nanoparticles have been extensively studied and have proven applications in diverse fields. Its applications range from antifungal treatments (Abdul *et al.* 2014; Kavyashree *et al*. 2015) and therapeutic transport systems (Yuan *et al*. 2010; Sharma and Ghose 2015) to antibacterial agents (Jones *et al*. 2008; Chen *et al*. 2013) and photo catalysts (Applerot *et al*. 2009; Banerjee *et al*. 2012). Given its remarkable properties and versatility, various synthesis techniques for zinc oxide, such as those reported in literature (Lee *et al*. 2016) have emerged.

The present study aims to synthesize zinc oxide nanomaterials via a green route using zinc acetate dihydrate and *Morinda citrifolia* leaf extract. As part of this study, Scanning Electron Microscopy (SEM) and Energy Dispersive X-ray (EDX) will be used to characterize the morphology and elemental composition of the prepared samples, and X-ray Diffraction (XRD) will be used to study their crystalline structure and

surface parameters. Optical and photoluminescence analyses will be carried out to assess their suitability for optoelectronic display applications. Additionally, the photocatalytic performance of the synthesized nanoparticles will be evaluated through solar-assisted degradation of Malachite Green dye, highlighting their potential for environmental remediation.

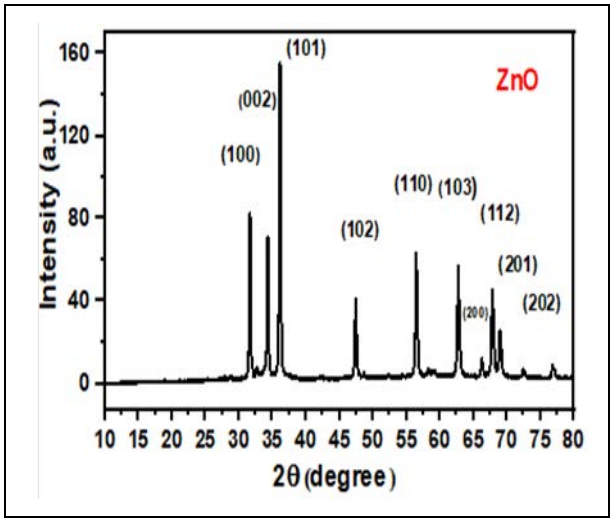


Fig. 2: X-ray diffraction patterns of the synthesized ZnO NPs

2. MATERIALS AND METHODS

2.1 Procurement of Plant Materials and Preparation of Leaf Extracts

The process commenced with the collection of *Morinda citrifolia* leaves, which were subsequently washed several times with distilled water. Then, the leaves were finely chopped into smaller pieces and dried at room temperature. About 12 g of chopped leaves are packed in packets and placed inside the Soxhlet extractor. The round-bottom flask is filled with 200 mL of ethanol. The apparatus is kept at 90 °C in a heating mantle till the complete extraction is over (2 hours).

2.2 Green Synthesis of ZnO Nanoparticles

Approximately 1.6425 g of zinc acetate was weighed and dissolved in 300 mL of distilled water in a beaker, followed by continuous stirring for 10 minutes. To this solution, 150 mL of plant extract and 150 mL of sodium hydroxide were gradually introduced under constant stirring at 650 rpm until the pH reached 12, which is considered optimal for ZnO precipitation and nanoparticle formation. Stirring was maintained for about 12 hours to ensure complete reaction. After settling, the mixture was distributed into conical flasks, each filled to 2/3 of its volume. The suspension was held in a thermostat-maintained water bath at 60°C with continuous agitation for 24–26 hours. After completion of the reaction, the ZnO nanoparticles were recovered by decantation or filtration, washed thoroughly, and stored for further characterization (Lee *et al.* 2016).

2.3 Characterization

The morphological analysis and size distribution of the prepared samples were conducted with a JSM 6360 model SEM, operating under the voltage of 200 kV. The elemental composition was examined through EDX performed with a QUANTA FEG 250 Analyzer. For examining the chemical structures of the prepared samples, FTIR spectroscopy was employed using a Bruker ALPHA FT-IR spectrometer. UV–Vis absorption spectra were recorded using a UV-2450 ultraviolet–visible spectrophotometer (Shimadzu, Japan).

3. RESULTS AND DISCUSSION

3.1 X-Ray Diffraction Studies

XRD serves as a versatile technique to analyze and examine the different crystalline structures and phases that are present in both powder and solid forms of samples.

XRD analysis displayed well-defined peaks indexed to the (100), (002), (101), (102), (110), (103), (200), (112), (201), and (202) crystallographic planes. These reflections are consistent with the hexagonal wurtzite structure of ZnO, in agreement with JCPDS card No. 36-1451. The dominant intensity along the (101) plane suggests a preferred orientation, which corresponds to the thermodynamically stable phase of ZnO. Additionally, the diffraction peak observed at a 2θ angle of approximately 37° corresponds to the (102) orientation of the wurtzite crystal structure of ZnO. The presence of sharp Bragg peaks suggests that the capping agent played a role in stabilizing the nanoparticles. The intensity of these Bragg reflections indicates a crystalline nature for the synthesized product. The broader peaks of solids detected in XRD patterns are associated with particle size effects. Wider peaks indicate reduced sizes of particles and show the impact of experimental conditions in the formation and growth of crystal nuclei. The crystallite size is responsible for this broadening effect, and the particle size of very small crystallites was calculated by using the Scherrer formula of Eqn. 1 based on the width of their diffraction peak.

$$D = \frac{0.94\lambda}{\beta\cos\theta} \quad \ldots (1)$$

where,

D is the average crystallite size,
λ represents the wavelength of X-rays,
β is the full width half maximum, and
θ is the angle of reflection.

The specific surface area of the sample was calculated from the formula (Ochieng *et al.* 2015),

$$S = \frac{6 \times 10^3}{\rho L} \quad \ldots (2)$$

where, S is the specific surface area (m^2/g), L is the average crystallite size, ρ is the density of the zinc oxide (5.606 g/cm^3) (Ochieng *et al.* 2015).

The crystallite size and surface area of the particle, calculated using Equations 1 and 2, are 29 nm and 36.9 m^2/g, respectively. It is noted that the increase in peak width decreases the particle size.

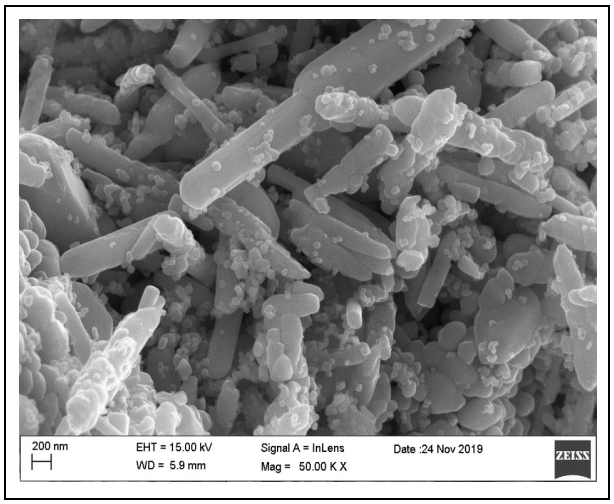


Fig. 3: Scanning Electron Micrograph of the eco-friendly synthesized ZnO NPs

3.2 SEM

Using a raster scan pattern, a high-energy electron beam is scanned to capture the surface morphological analysis of the samples by SEM. The surface analysis of the developed ZnO nanorods was assessed through SEM, as shown in Fig. 3. The analysis revealed that the nanorods possess an average dimension of nearly 193.78 nm and an average diameter of about 31.78 nm. Noticeable agglomeration was observed, which can be ascribed to the intrinsic polar nature and electrostatic interactions of ZnO nanoparticles. This behavior arises from the wurtzite crystal structure of ZnO, characterized by alternating layers of zinc cations (Zn^{2+}) and oxide anions (O^{2-}) along the c-axis, resulting in a polar nature that promotes particle aggregation. This polar structure creates dipole moments on the nanoparticle surfaces, leading to strong electrostatic interactions between particles. Additionally, at the nanoscale, the high surface energy & unsatisfied surface charges of ZnO nanorods promote Van der Waals forces and Columbic interactions, further enhancing the tendency of individual nanoparticles to cluster together. As a result, these electrostatic and polar effects lead to the formation of agglomerates in the ZnO nanoparticle system.

3.3 EDX

The EDX disclosed the existence of four peaks within the 1 to 10 keV range, affirming the presence of Zn, with a clear peak observed at 1 keV (Fig. 4.). The EDX spectra further affirmed the existence of the necessary phases of Zn and O in the developed samples, attesting to the purity of the produced nanoparticles of zinc (Zn NPs). The stoichiometric mass percentages of Zn and O were identified to be 80.3% and 19.7%, respectively.

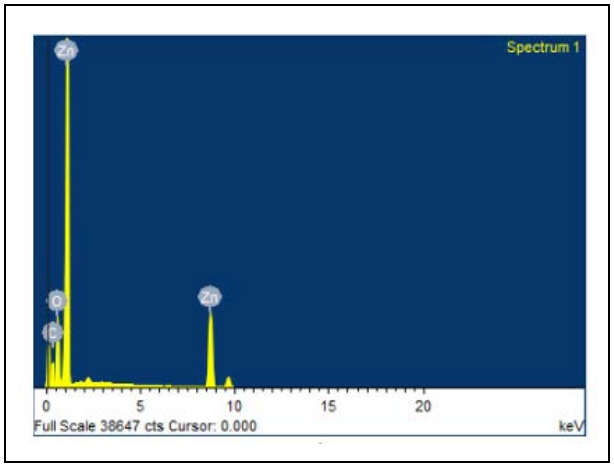


Fig. 4: EDAX Spectrum of the eco-friendly synthesized ZnO NPs

3.4 FT-IR Spectral Analysis

FT-IR studies of the produced ZnO nanoparticles are depicted in Fig. 5. These infrared investigations help to evaluate the characteristics and purity of the sample nanoparticles as well as to look for phytochemicals in the extract. A variety of phytochemicals, including carboxylic acids, amines, phenols, and alcohols, may interact with the surface of zinc to stabilize nanoparticles of zinc oxide.

The stretching and deformation vibrations of ZnO correspond to the peaks observed at 1634 cm^{-1}, 831 cm^{-1}, and 432 cm^{-1}, which are attributed to different vibrational modes associated with the Zn–O bond and its surface interactions. The peak observed at 1634 cm^{-1} can be ascribed to O–H bending vibrations resulting from surface hydroxyl groups and physically adsorbed water on ZnO nanoparticles. The absorption band at 831 cm^{-1} corresponds to Zn–O stretching vibrations within a slightly distorted tetrahedral coordination, typical of the ZnO wurtzite structure. Additionally, the dominant low-frequency peak at 432 cm^{-1} is characteristic of Zn–O stretching, serving as direct confirmation of ZnO phase formation.

The absorption maxima of the metal-oxide typically fall in the 600–400 cm^{-1} range. This confirms the production of the ZnO phase and supports the presence of Zn–O bonding in the wurtzite crystal lattice. Its position and intensity are consistent with literature-reported ZnO nanoparticles, confirming the purity and successful synthesis of the oxide (Rao *et al.* 2015; Singh *et al*. 2011).

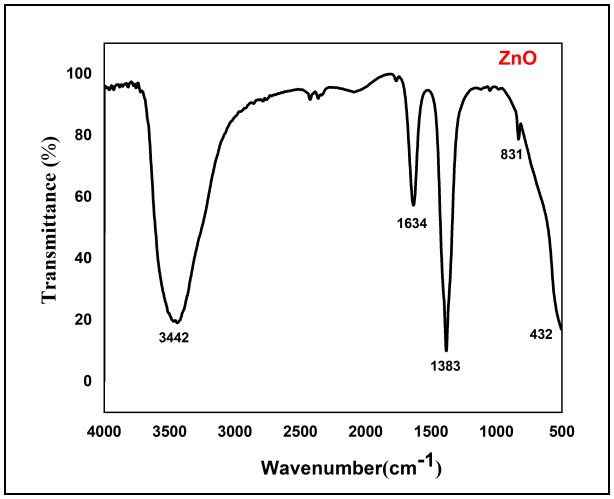


Fig. 5: FTIR spectra of the synthesized ZnO NPs

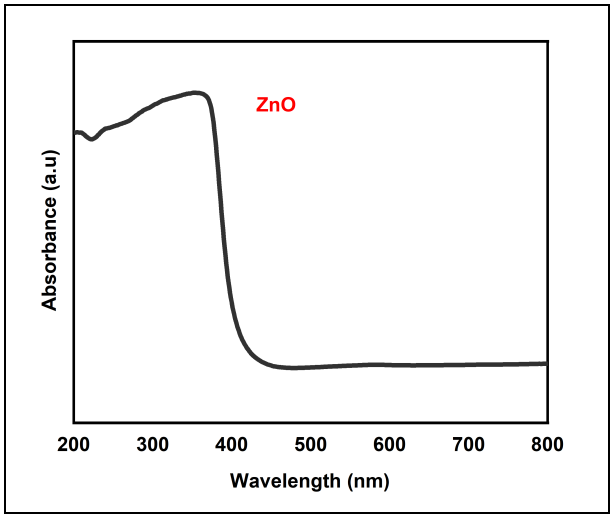


Fig. 6(a): UV-Visible spectrum of the synthesized ZnO NPs

3.5 Ultraviolet-Visible Spectroscopy

A distinctive peak, positioned at 350 nm, is observed, characteristic of zinc oxide nanorods and attributed to their substantial excitation binding energy at room temperature (Rao *et al.* 2015). According to absorption spectroscopy principles, the bandgap tends to increase with decreasing particle size. In this case, the sample exhibits an optical absorption peak at 400 nm, which slowly decreases at higher wavelengths (Fig. 6(a)). Notably, there are no other secondary peaks that are detected in the spectrum, which confirms the exclusive presence of synthesized ZnO nanoparticles. Zinc oxide NPs are known to display a characteristic broad absorption spectrum between 330-460 nm (Bhuyan *et al.* 2015). Thus, the optical absorption band around 400 nm serves as confirmation of the successful production of ZnO nanoparticles.

Using Tauc's equation $(\alpha h\nu)^n = A\ (h\nu - Eg)$, the band gap values were derived by plotting $(\alpha h\nu)^2$ against $h\nu$ and extending the linear section to the energy axis.

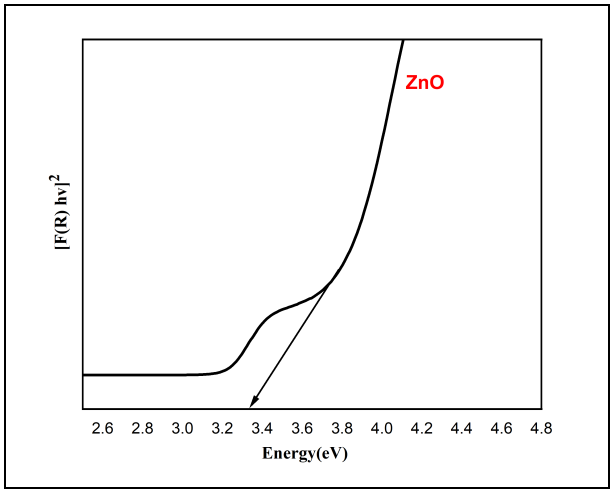


Fig. 6(b): Band gap spectrum of the synthesized ZnO NPs

The band gap (optical) value of ZnO was shown in Fig. 6(b) as 3.36 eV. A slight variation in band gap indicates nano-crystallinity and effective synthesis.

3.6 Photoluminescence (PL) Analysis

A photoluminescence spectrometer recorded the photoluminescence (PL) spectra at room temperature using a He-Cd laser operating at 325 nm as the light source. The sample spectrum shows the presence of two different peaks: a broad visible light emission from about 300 nm to 500 nm, complemented by a weak defect emission peak of about 500 nm (orange emission), and a weak (UV) ultraviolet emission spectrum at about 410 nm. The near band edge emission (NBE) in ZnO's large band gap is responsible for the UV emission at 387.5 nm. This emission is linked to exciton-related activity and is the result of direct recombination of photogenerated charge carriers (Nagarajan and Arumugam Kuppusamy 2013). Particularly, the quantum confinement effect causes electrons in smaller particles with a wide band gap to become excited to the conduction band (CB) when exposed to shorter wavelength light. As the deep levels of defects remain unaltered, the relaxation of electrons from the conduction band to the defect levels emits photons of large energy, corresponding to a shorter wavelength. As the excitation wavelength increases, electrons in larger particles are found to be exclusively excited. Those larger particles have a band gap that is

close to that of bulk amorphous zinc oxide, causing the emitted light to have a longer wavelength. Consequently, the emission wavelength red shifts with an increase in the excitation wavelength. The photoluminescence results corroborate the quantum confinement and defect-mediated emission phenomena in ZnO NPs. A comparison with prior research affirms the presence of oxygen- and zinc-related intrinsic defects, which are likely influenced by the green synthesis method employed.

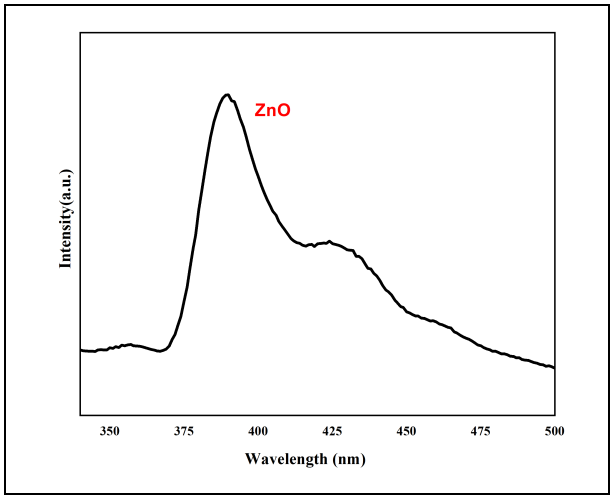


Fig. 7: Photoluminescence spectra (PL) of the synthesized ZnO NPs

3.7 Sunlight-driven Photocatalytic Degradation Studies

The photocatalytic capability of ZnO nanoparticles was examined by Malachite Green dye as a representative pollutant, with 10 mg of ZnO dispersed in 100 mL of a 10 mg/L solution for each trial. A concentration of 10 mg/L was chosen based on existing literature reports and preliminary trials that indicate this range effectively enhances photocatalytic activity without inducing significant light scattering or agglomeration of nanoparticles. To ensure adsorption–desorption equilibrium, the samples were stirred magnetically in the dark for 30 minutes before the photocatalytic experiment. The subsequent photodegradation experiments were conducted in a reactor equipped with a water-jacket system, which maintained the reaction mixture at a stable temperature through continuous water circulation. UV–Vis absorption spectra obtained using a UV–Vis spectrophotometer were used to determine the dye concentration. The photocatalytic degradation efficiency of the dye was determined using Eqn. 3:

$$\text{Degradation efficiency} = \frac{C_0 - C}{C_0} \times 100\% \quad \ldots (3)$$

where, C_o and C are the initial dye concentration of the solution before illumination and the residual concentration after illumination for different time intervals (0, 10, 20, 30, 40, 50, and 60 minutes).

Malachite green (MG) undergoes ionization to generate an intermediate state, MG, and oxalate ion. The degradation pathway of Malachite Green (MG) involves the attack of reactive free radicals on its chromophore ring, resulting in ring cleavage and the generation of intermediate mineral acids. This sequential process ultimately results in a visible color change from blue to a nearly colorless solution (Nagarajan and Arumugam Kuppusamy 2013; Jie *et al.* 2022). The present study demonstrated a notable degradation efficiency exceeding 90%, indicating the potential suitability of ZnO nanoparticles for environmental remediation compared to other photocatalytic materials used for the photocatalytic degradation of Malachite green (MG) with a rate constant of 0.0337 min^{-1}. For comparison, ZnO NPs produced utilizing green synthesis by *Justicia adhatoda* achieved a degradation efficiency of 99.8% using 100 mg/L of ZnO and 10 mg/L of MG under UV and sunlight irradiation for 180 minutes (Saikia *et al.* 2015; Jeevanantham *et al.* 2023; Mahajan *et al.* 2025).

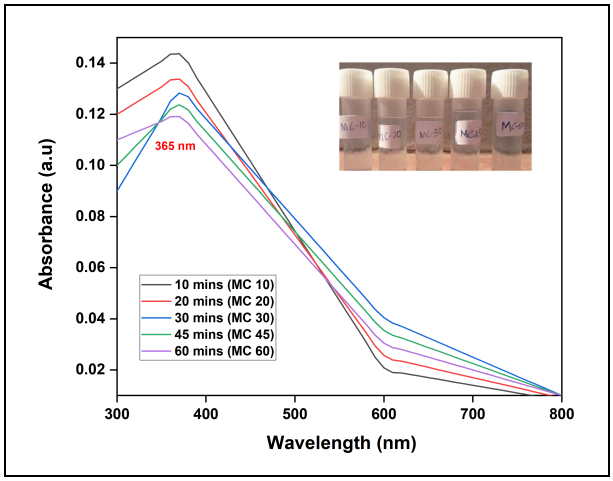


Fig. 8: Photocatalytic degradation of Malachite Green by ZnO nano-photocatalyst

4. CONCLUSION

Using *Morinda citrifolia* leaf extract and zinc acetate dihydrate as eco-friendly precursors, ZnO nanoparticles were green-synthesized. The XRD patterns of ZnO nanoparticles matched the hexagonal wurtzite phase as referenced in JCPDS No. 36-1451. The diffraction peaks exhibited sharpness and strength, indicating high crystal quality and a particle size on the order of approximately 29 nm. SEM images illustrated the surface morphological image of the as-prepared zinc oxide nanoparticles, appearing as clusters of nanorods. EDX results exhibited peaks corresponding exclusively to zinc and oxygen elements, affirming the purity of the samples. FT-IR analysis of the nano-ZnO clusters confirmed the presence of metal oxide peaks and verified

the absence of any unreacted precursors. The UV-Vis absorption spectrum displayed a broad absorption peak throughout the UV region, suggesting the material's suitability for blocking UV radiation. Photoluminescent spectra revealed a blue-green band at 491 nm, indicating potential applications for display purposes in optoelectronic devices. Notably, the photocatalytic efficiency exceeded 90%, highlighting its effectiveness for environmental remediation.

FUNDING

This research received no specific grant from any funding agency in the public, commercial, or not-for-profit sectors.

CONFLICT OF INTEREST

The authors declared no conflict of interest in this manuscript regarding publication.

COPYRIGHT

This article is an open-access article distributed under the terms and conditions of the Creative Commons Attribution (CC BY) license (http://creativecommons.org/licenses/by/4.0/).



REFERENCES

Amna, S., Shahrom, M., Azman, S., Noor, H., Mohamad, Kaus, L., Chuo, A., Siti, K. M. B., Habsah, H. and Dasmawati, M., Review on Zinc Oxide Nanoparticles: Antibacterial Activity and Toxicity Mechanism, *Nano-Micro Lett.*, 7(3), 219–242, (2015). https://doi.org/10.1007/s40820-015-0040-x

Ahmed, S., Ahmad, M., Swami, B. L. and Ikram, S., A review on plants extracts mediated synthesis of silver nanoparticles for antimicrobial applications: A green expertise, *J. Adv. Res.*, 7(1), 17–28 (2016). https://doi.org/10.1016/j.jare.2015.02.007

Al-darwesh, M. Y., Ibrahim, S. S. and Mohammed, M. A., A review on plant extract mediated green synthesis of zinc oxide nanoparticles and their biomedical applications, *Results Chem.*, 7101368 (2024). https://doi.org/10.1016/j.rechem.2024.101368

Applerot, G., Lipovsky, A., Dror, R., Perkas, N., Nitzan, Y., Lubart, R. and Gedanken, A., Enhanced Antibacterial Activity of Nanocrystalline ZnO Due to Increased ROS-Mediated Cell Injury, *Adv. Funct. Mater.*, 19(6), 842–852 (2009). https://doi.org/10.1002/adfm.200801081

Banerjee, P., Chakrabarti, S., Maitra, S. and Dutta, B. K., Zinc oxide nano-particles – Sonochemical synthesis, characterization and application for photo-remediation of heavy metal, *Ultrason. Sonochem.*, 19(1), 85–93 (2012). https://doi.org/10.1016/j.ultsonch.2011.05.007

Bhuyan, T., Mishra, K., Khanuja, M., Prasad, R. and Varma, A., Biosynthesis of zinc oxide nanoparticles from Azadirachta indica for antibacterial and photocatalytic applications, *Mater. Sci. Semicond. Process.*, 3255–61 (2015). https://doi.org/10.1016/j.mssp.2014.12.053

Chen, T., Zhao, T., Wei, D., Wei, Y., Li, Y., and Zhang, H., Core–shell nanocarriers with ZnO quantum dots-conjugated Au nanoparticle for tumor-targeted drug delivery, *Carbohydr. Polym.*, 92(2), 1124–1132 (2013). https://doi.org/10.1016/j.carbpol.2012.10.022

Divya, P. and Nithya, T., Silver Nanoparticles Eco-Friendly Synthesis by ornamental flower extracts and evaluation of their antimicrobial activity, *Int. J. of Res. in Pharm. and Nano Sci.*, 4(4), 250-259 (2015).

Dong, H., Zeng, G., Tang, L., Fan, C., Zhang, C., He, X. and He, Y., An overview on limitations of TiO2-based particles for photocatalytic degradation of organic pollutants and the corresponding countermeasures, *Water Res.*, 79, 128–146 (2015). https://doi.org/10.1016/j.watres.2015.04.038

Jie, T., Zhifeng, L., Jie, L., Yuan, M., Xiaolong, Y., Yu hui, W., Yong, L. and Tingting, Z., Visible-light-assisted peroxymonosulfate activation by metal-free bifunctional oxygen-doped graphitic carbon nitride for enhanced degradation of imidacloprid: Role of non-photochemical and photocatalytic activation pathway, *J. Hazard. Mater.*, 423, 127048, (2022). https://doi.org/10.1016/j.jhazmat.2021.127048

Jo, W. K. and Tayade, R. J., Recent developments in photocatalytic dye degradation upon irradiation with energy-efficient light emitting diodes, *Chin. J. Catal.*, 35(11), 1781–1792 (2014). https://doi.org/10.1016/S1872-2067(14)60205-9

Jones, N., Ray, B., Ranjit, K.T. and Manna, A. C., Antibacterial activity of ZnO nanoparticle suspensions on a broad spectrum of microorganisms, *FEMS Microbiol. Lett.*, 279(1), 71–76 (2008). https://doi.org/10.1111/j.1574-6968.2007.01012.x

Heinicke, R. M., *Xeronine, a new alkaloid, useful in medical, food and industrial fields*. U.S. Patent No. 4, 543,212 (1985).

Kalpana, V. N. and Devi Rajeswari, V., A Review on Green Synthesis, Biomedical Applications, and Toxicity Studies of ZnO NPs, *Bioinorg. Chem. Appl.*, 20181–12 (2018). https://doi.org/10.1155/2018/3569758

Kavyashree, D., Shilpa, C. J., Nagabhushana, H., Daruka Prasad, B., Sreelatha, G.L., Sharma, S.C., Ashoka, S., Anandakumari, R. and Premkumar, H.B., ZnO Superstructures as Antifungal for Effective Control of *Malassezia furfur*, Dermatologically Prevalent Yeast: Prepared by Aloe Vera Assisted Combustion Method, *ACS Sustain. Chem. Eng.*, 3(6), 1066–1080 (2015). https://doi.org/10.1021/sc500784p

Kavitha, T., Gopalan, A. I., Lee, K. P. and Park, S. Y., Glucose sensing, photocatalytic and antibacterial properties of graphene–ZnO nanoparticle hybrids, *Carbon*, 50(8), 2994–3000,(2012). https://doi.org/10.1016/j.carbon.2012.02.082

Lee, K. M., Lai, C.W., Ngai, K. S. and Juan, J. C., Recent developments of zinc oxide based photocatalyst in water treatment technology: A review, *Water Res.*, 88428–448 (2016). https://doi.org/10.1016/j.watres.2015.09.045

Mahajan, M., Kumar, S., Gaur, J., Kaushal, S., Dalal, J., Singh, G., Misra, M., & Ahlawat, D. S. Green synthesis of ZnO nanoparticles using *Justicia adhatoda* for photocatalytic degradation of malachite green and reduction of 4-nitrophenol. *RSC Advances*, 15(4), 2958–2980, (2025). https://doi.org/10.1039/D4RA08632E

Makarov, V. V., Love, A. J., Sinitsyna, O. V., Makarova, S.S., Yaminsky, I.V., Taliansky, M.E., and Kalinina, N. O., "Green" Nanotechnologies: Synthesis of Metal Nanoparticles Using Plants, *Acta Naturae*, 6(1), 35–44 (2014). https://doi.org/10.32607/20758251-2014-6-1-35-44

Malik, P., Shankar, R., Malik, V., Sharma, N. and Mukherjee, T.K., Green Chemistry Based Benign Routes for Nanoparticle Synthesis, *J. Nanoparticles*, 20141–14 (2014). https://doi.org/10.1155/2014/302429

Mittal, A. K., Chisti, Y., and Banerjee, U. C., Synthesis of metallic nanoparticles using plant extracts, *Biotechnol. Adv.*, 31(2), 346–356 (2013). https://doi.org/10.1016/j.biotechadv.2013.01.003

Rao, M. V., Muthukrishnan, S., Bhakya, S., Senthil, K. T., Biosynthesis, characterization and antibacterial effect of plant-mediated silver nanoparticles using *Ceropegia thwaitesii* – An endemic species, *Ind. Crops Prod.*, 63, 119-124 (2015). https://doi.org/10.1016/j.indcrop.2014.10.022

Nagarajan, S. and Arumugam, K. K., Extracellular synthesis of zinc oxide nanoparticle using seaweeds of Gulf of Mannar, India, *J. Nanobiotechnology*, 11(1), 39 (2013). https://doi.org/10.1186/1477-3155-11-39

Ochieng P. E., E. Iwuoha, I. Michira, M. Masikini, J. Ondiek, P. Githiraand G. N. Kamau, green route synthesis and characterization of zno nanoparticles using spathodeacampanulata, *Int. J. of BioChemiPhysics*, 53-61, 23,(2015).

Singh, P., Shukla, R., K., Yadav, V., S., Sharma, R., K., Singh, P., K. P. and Pandey, A. C., Biological approach of zinc oxide nanoparticles formation and its characterization, *Adv. Mater. Lett.*, 2(4), 313–317 (2011). https://doi.org/10.5185/amlett.indias.204

Ramesh, M., Anbuvannan, M., and Viruthagiri, G., Green synthesis of ZnO nanoparticles using Solanum nigrum leaf extract and their antibacterial activity, *Spectrochim. Acta. A. Mol. Biomol. Spectrosc.*, 136864–870 (2015). https://doi.org/10.1016/j.saa.2014.09.105

Saikia, L., Bhuyan, D., Saikia, M., Malakar, B., Dutta, D. K. and Sengupta, P. Photocatalytic performance of ZnO nanomaterials for self-sensitized degradation of malachite green dye under solar light. *Applied Catalysis A: General*, 490, 42–49 (2015). https://doi.org/10.1016/j.apcata.2014.10.051

Sharma, R.K. and Ghose, R., Synthesis of zinc oxide nanoparticles by homogeneous precipitation method and its application in antifungal activity against Candida albicans, *Ceram. Int.*, 41(1), 967–975 (2015). https://doi.org/10.1016/j.ceramint.2014.09.016

Shengmin, S., Mingfu, W., Kan, H., Guangming, L., Zigang, D., Vladimir, B., Qun, Y. Z., Geetha, G., Robert, T. R. and Chi-Tang, H., Chemical Components in Noni Fruits and Leaves (*Morinda citrifolia* L.), *Am. Chem. Soc.*, 134-150, (2002). https://doi.org/:10.1021/bk-2002-0803.ch010

Sushma, N. J., Mahitha, B., Mallikarjuna, K. B. and Deva, P. B., Bio-inspired ZnO nanoparticles from Ocimum tenuiflorum and their in vitro antioxidant activity, *Appl. Phys. A*, 122, 544 (2016). https://doi.org/10.1007/s00339-016-0069-9

Jeevanantham, V., Tamilselvi, D., Bavaji, S. R. and Mohan, S., Green formulation of gold nanoparticles and their antioxidative assays, antimicrobial activity and photocatalytic colour decay, *Bull. Mater. Sci. Indian Academy Sci.*, 46, 32 (2023). https://doi.org/10.1007/s12034-022-02868-1

Vivek, E., Senthilkumar, N., Pramothkumar, A., Vimalan, M. and Potheher, I.V., Synthesis of flower-like copper oxide microstructure and its photocatalytic property, *Phys. B Condens. Matter*, 56696–102 (2019). https://doi.org/10.1016/j.physb.2019.05.009

Wan, C., Zhou, L., Sun, L., Xu, L., Cheng, D., Chen, F., Zhan, X. and Yang, Y., Boosting visible-light-driven hydrogen evolution from formic acid over AgPd/2D g-C3N4 nanosheets Mott-Schottky photocatalyst, *Chem. Eng. J.*, 396125229 (2020). https://doi.org/10.1016/j.cej.2020.125229

Yuan, Q., Hein, S. and Misra, R.D.K., New generation of chitosan-encapsulated ZnO quantum dots loaded with drug: Synthesis, characterization and in vitro drug delivery response, *Acta Biomater.*, 6(7), 2732–2739 (2010). https://doi.org/10.1016/j.actbio.2010.01.025